Bioorganic & Medicinal Chemistry Letters 30 (2020) 127632

Contents lists available at ScienceDirect

Bioorganic & Medicinal Chemistry Letters

journal homepage: www.elsevier.com/locate/bmcl

The optimization of a novel selective antagonist for human M_2 muscarinic acetylcholine receptor

Miaomiao Li[a,h], Chen Huang[b,c,h], Xingyu Wu[d], Fan Ding[b], Zhoumi Hu[b], Yan Zhu[e], Lanxue Zhao[a], Lina Hou[a], Hongzhuan Chen[a,f], Hao Wang[a], Jianrong Xu[a,g,*], Dewei Tang[b,*]

[a] Department of Pharmacology and Chemical Biology, Shanghai Jiao Tong University School of Medicine, Shanghai, 200025, China
[b] Department of Nuclear Medicine, Renji Hospital, School of Medicine, Shanghai Jiao Tong University, 160 Pu Jian Road, Shanghai 200127, China
[c] College of Medical Imaging, Shanghai University of Medicine and Health Sciences, Shanghai 201318, China
[d] College of Pharmacy, Shanghai University of Medicine and Health Sciences, Shanghai 201318, China
[e] School of Medical Instrument and Food Engineering, University of Shanghai for Science and Technology, Shanghai 200093, China
[f] Institute of Interdisciplinary Integrative Biomedical Research, Shanghai University of Traditional Chinese Medicine, Shanghai 201203, China
[g] Academy of Integrative Medicine, Shanghai University of Traditional Chinese Medicine, Shanghai 201203, China

ARTICLE INFO

Keywords:
Muscarinic acetylcholine receptor
Antagonist
Structure–activity relationship
Selective
Alzheimer's disease

ABSTRACT

Muscarinic acetylcholine receptors (mAChRs) comprise five distinct subtypes denoted M_1 to M_5. The antagonism of M_2 subtype could increase the release of acetylcholine from vesicles into the synaptic cleft and improve postsynaptic functions in the hippocampus *via* M_1 receptor activation, displaying therapeutic potentials for Alzheimer's disease. However, drug development for M_2 antagonists is still challenged among different receptor subtypes. In this study, by optimizing a scaffold from virtual screening, we synthesized two focused libraries and generated up to 50 derivatives. By measuring potency and binding selectivity, we discovered a novel M_2 antagonist, ligand **47**, featuring submicromolar IC_{50}, high M_2/M_4 selectivity (~30-fold) and suitable lipophilicity (cLogP = 4.55). Further study with these compounds also illustrates the structure–activity relationship of this novel scaffold. Our study could not only provide novel lead structure, which was easy to synthesize, but also offer valuable information for further development of selective M_2 ligands.

G protein-coupled receptors (GPCRs) constitute the largest family of proteins targeted by Food and Drug Administration approved drugs.[1] The muscarinic acetylcholine receptors (mAChRs) belong to α-branch of class A GPCRs and they are ubiquitously distributed in human organs, regulating a variety of physiological functions including heartbeats, smooth muscle contraction, glandular secretion and many fundamental functions for central nervous system (CNS).[2] mAChRs comprise five distinct subtypes denoted M_1 to M_5. Three of these subtypes (M_1, M_3 and M_5) are coupled to G proteins of the $G_{q/11}$ family, while the other two subtypes (M_2 and M_4) are coupled to G proteins of the $G_{i/o}$ family.[3] Currently, drugs targeting mAChRs are generally developed for the treatment of various diseases, including chronic obstructive pulmonary diseases, Alzheimer's disease, Parkinson's disease, overactive bladder syndromes and other diseases like cancer, diabetes, cardiovascular diseases, pain and inflammation.[3–5]

M_1 to M_5 subtypes feature different tissue distribution patterns in human. For example, M_1, M_2 and M_4 subtypes are the major mAChRs subtypes expressed in the brain, where M_3 and M_5 subtypes are expressed at significantly lower levels.[6] In neurons, the M_2 subtype is the largely presynaptic receptor associated with axons and inhibits neuronal excitability, which results in the negative feedback of neurotransmitter release.[7] At synapses, the antagonism of the M_2 subtype could increase the release of acetylcholine (ACh) from vesicles into the synaptic cleft and improve postsynaptic functions in the hippocampus

Abbreviations: mAChRs, muscarinic acetylcholine receptors; GPCRs, G protein-coupled receptors; CNS, central nervous system; GIRK, G protein-coupled inwardly rectifying K^+ channels; ACh, acetylcholine; PAM, positive allosteric modulator; BQCA, benzyl quinolone carboxylic acid; NAM, negative allosteric modulator; BBB, blood-brain barrier; SARs, structure-activity relationships; LOO, leave-one-out; QSAR, quantitative structure-activity relationships; QNB, quinuclidinyl benzylate; SP, standard precision

* Corresponding authors at: Department of Pharmacology and Chemical Biology, Shanghai Jiao Tong University School of Medicine, Shanghai, 200025, China and Academy of Integrative Medicine, Shanghai University of Traditional Chinese Medicine, Shanghai 201203, China (J. Xu) and Department of Nuclear Medicine, Renji Hospital, School of Medicine, Shanghai Jiao Tong University, 160 Pu Jian Road, Shanghai 200127, China (D. Tang).
E-mail addresses: janker.xu@gmail.com (J. Xu), acetdw@126.com (D. Tang).
[h] These authors contributed equally to this work.

https://doi.org/10.1016/j.bmcl.2020.127632
Received 31 July 2020; Received in revised form 14 October 2020; Accepted 16 October 2020
Available online 24 October 2020
0960-894X/

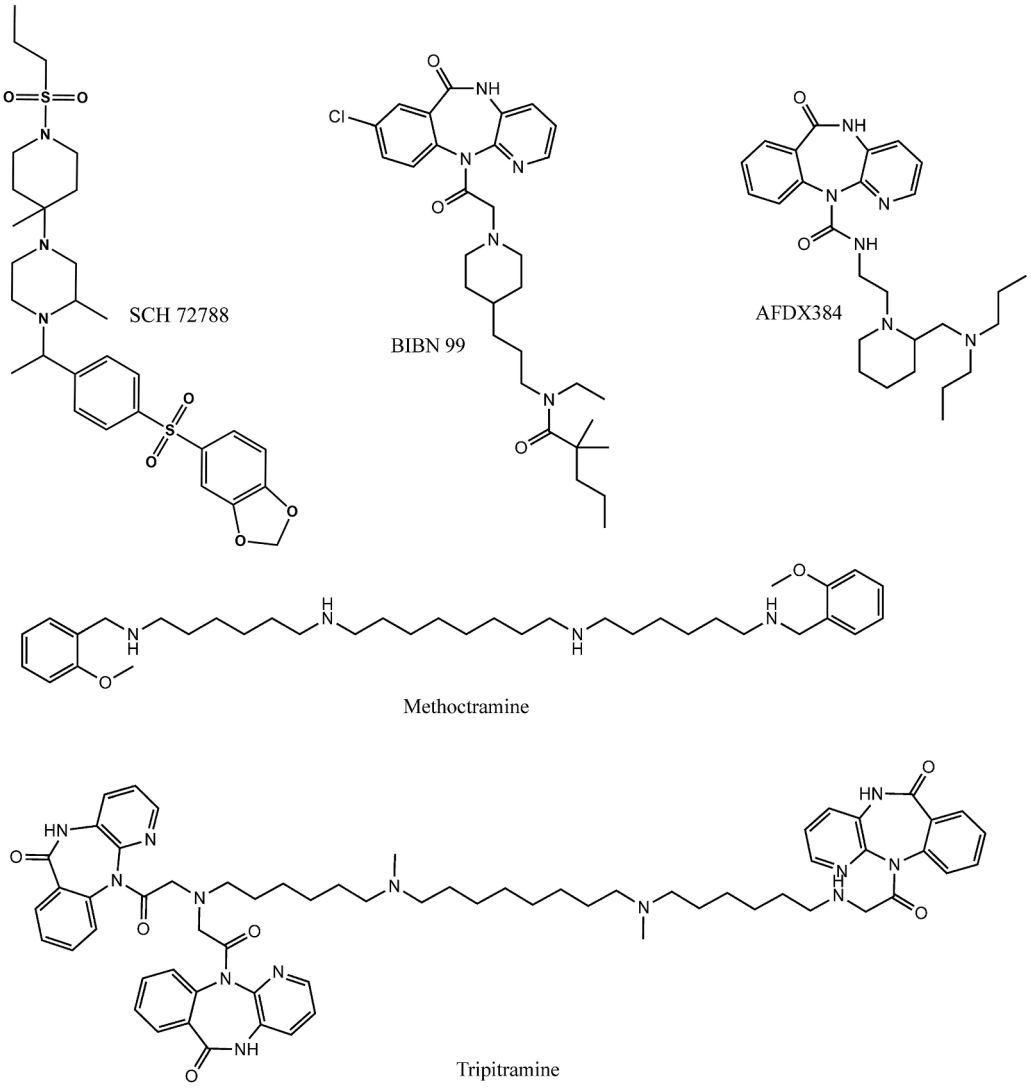

Fig. 1. The structures of M_2 subtype antagonists.

via M_1 subtype activation, displaying therapeutical potentials for Alzheimer's disease.[4,8–11]

Human M_1 to M_5 subtypes share 64 to 82% sequence identity and 82 to 92% sequence similarity in the transmembrane region, but they vary significantly at the *N*-terminal and extracellular regions. Although M_2 receptor is an attractive target for Alzheimer's disease, it is still challenging to discover novel subtype-specific ligands. By using allosteric strategy, several subtype-selective mAChRs ligands have been successfully developed, such as the M_1 subtype positive allosteric modulator (PAM) benzyl quinolone carboxylic acid (BQCA) , and the M_5 receptor negative allosteric modulator (NAM) ML375.[12,13] Despite significant progress through these strategies, the orthosteric site still showed valuable potentials for subtype-selective ligands, such as the latest achievements on both M2 and M3 subtypes.[14–17]

Currently, several antagonists for M_2 mAChRs like SCH 72,788,[18] BIBN[19,20] and AFDX384[15,21,22] have been developed (Fig. 1), but are still limited on their M_2/M_4 selectivity. Other two M_2 specific antagonists, methoctramine[23–25] and tripitramine[26–28], with cLogP values larger than 7, are also limited in their ability to cross the blood–brain barrier (BBB) (Fig. 1). Therefore, there is still an urgent need to develop novel antagonists for M_2 subtype with high selectivity, binding affinity, drug potential and suitable lipophilicity ($3 < \text{cLogP} < 5$).

At present, the structures of mAChRs have been determined using X-ray crystallography and Cryo-EM, providing new opportunities for the discovery of subtype-selective ligands.[29–34] Novel selective M_2 antagonists can be developed based on these structures and the structure–activity relationships (SARs). In this study, by optimizing from a non-selective antagonist with a novel scaffold obtained from virtual screen, we performed a two-round optimization and synthesized up to 50 different derivatives. By measuring the binding specificity and drug potential of each compound, we discovered a novel M_2 antagonist featuring a high M_2/M_4 selectivity, suitable lipophilicity as well as the drug potentials. Further SARs have also been elucidated with the focused library developed in this research.

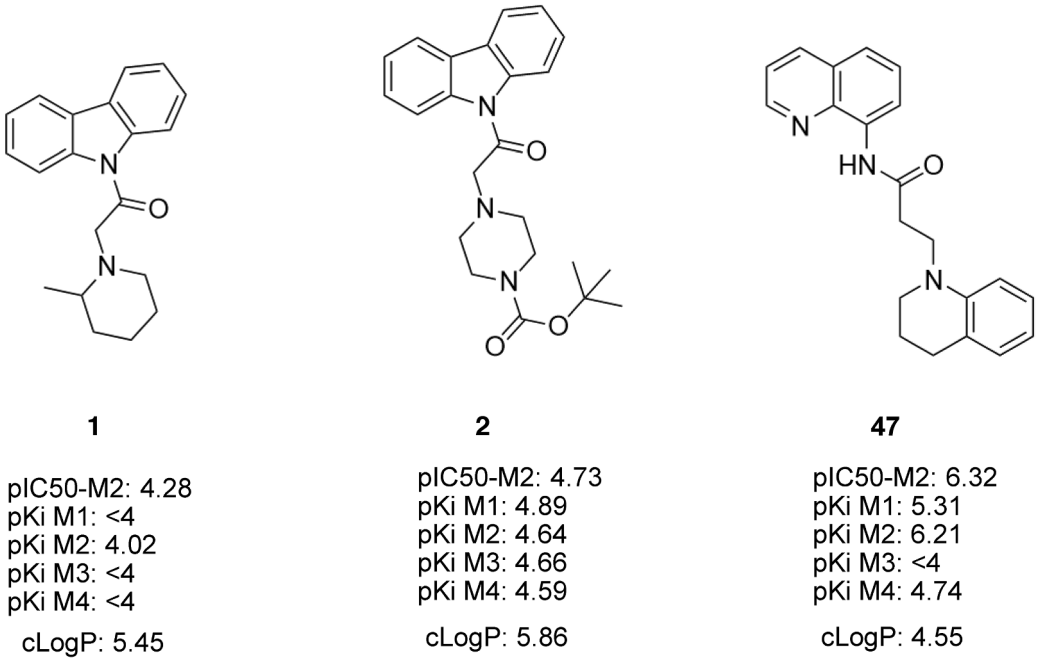

Fig. 2. Structure, activities and cLogP of lead compound **1**, **2** and **47**.

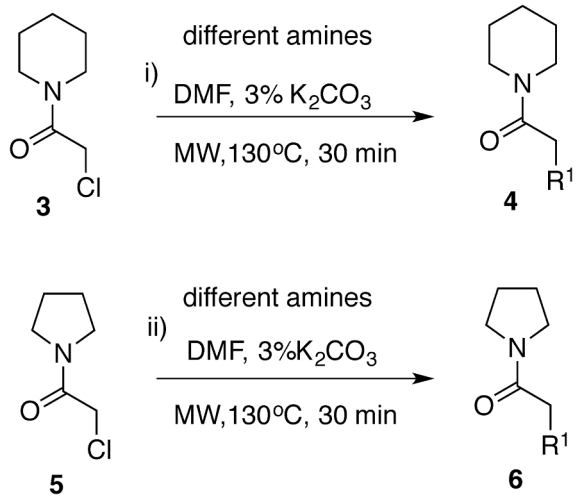

Scheme 1. Synthetic approach for the ligand optimization to setup the focused library 1. i) different amines, DMF (3% K_2CO_3), 130 °C, 30 min; ii) different amines, DMF(3% K_2CO_3), 130 °C, 30 min.

By using Glide module in Schrodinger, this study screened 1.5 million compounds in commercial databases, including SPECS and Chemdiv. The first-round screening was ranked by G score and the top 10,000 compounds were reranked under extra precision mode. Based on CHO-K1/M2/Gα15 cell line, Ca^{2+} mobilization assay was applied for the top 184 compounds in the ranking, of which 66 compounds were purchased from SPECS and 118 compounds were from Chemdiv. Five of them were identified as agonists of M_2 receptors, such as AG-205–6. However, only AJ-292 (lead compound **1**) in SPECS database was characterized to be an antagonist at high concentration. Because AJ-292 showed a novel scaffold for mAChRs antagonists and had various sites for further optimization, we took it as the lead and carried out the following optimization.

IC_{50} is a quantitative measure that indicates how much of a particular inhibitory substance is needed to inhibit a given biological process by 50% and here refers to the potency to antagonize functional response to the agonist ACh on mAChRs. In this study, by optimizing the lead compound **1**, we synthesized up to 50 compounds and measured the binding affinity and specificity for each compound. The lead compound features a scaffold comprising a carbazole and a piperidine ring. A simple modification on the piperidine ring produced the compound **2**, which did not show a dramatic IC_{50} increase when compared to parent compound **1** (Fig. 2). In order to discover the novel ligand with higher IC_{50} and a suitable lipophilicity, an initial optimization was performed to investigate the role of carbazole for the drug potential, by using different two-ring amines as shown in Scheme 1 and Table 1. With this optimization, two desired compounds **11** and **17** was discovered. Both of these two ligands have a submicromolar IC_{50} and increased binding affinities for M_1 to M_4 subtypes when compared to the parent compound **1**.

Interestingly, the modification from the carbazole to tetrahydroquinoline dramatically improve the IC_{50} by more than 100 fold, as indicated by the IC_{50} of **1**, **11** and **17**. On the other side, the optimization using indoline did not yield the higher potential ligands as tetrahydroquinoline, as indicated by the comparison between **7**, **8**, **15**, **18** and **9**, **10**, **11**, **14**, **16**, **17.** Similarly, substitution of tetrahydroquinoline with tetrahydronaphthyridine will also lower the scaffold binding affinity to all the four subtypes of mAChRs, as indicated by the comparison between **11**, **17** and **13**, **19** in Table 1. Interestingly, the simple substitution of piperidine with pyrrolidine in the scaffold did not affect the IC_{50} significantly as shown in Table 1 by the direct

Table 1

Structure and activity of the focused library 1.

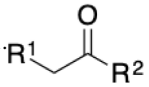

Entry	R^1	R^2	pIC50 M2	pKi M1	pKi M2	pKi M3	pKi M4	cLogP
1	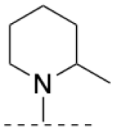	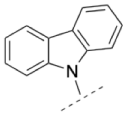	4.28 ± 0.08	< 4	4.02 ± 0.08	< 4	< 4	5.45
2	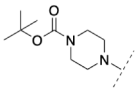	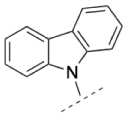	4.73 ± 0.01	4.89 ± 0.05	4.64 ± 0.05	4.66 ± 0.12	4.59 ± 0.06	5.86
7	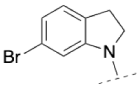	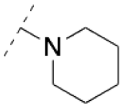	< 4	< 4	< 4	< 4	< 4	3.86
8	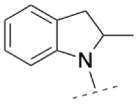	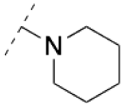	< 4	NA	< 4	< 4	< 4	3.35
9	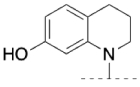	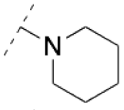	5.03 ± 0.05	< 4	4.39 ± 0.06	< 4	4.06 ± 0.08	2.57
10	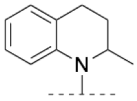	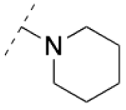	5.13 ± 0.06	4.55 ± 0.07	5.44 ± 0.07	4.28 ± 0.08	5.05 ± 0.07	3.76
11	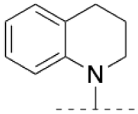	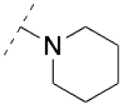	6.36 ± 0.06	5.54 ± 0.06	6.38 ± 0.08	4.96 ± 0.07	5.91 ± 0.07	3.33
12	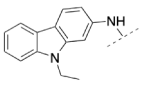	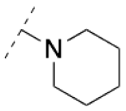	5.01 ± 0.05	4.36 ± 0.09	4.31 ± 0.28	4.35 ± 0.10	4.04 ± 0.08	4.49
13	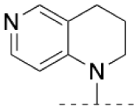	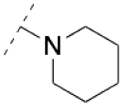	< 4	< 4	4.39 ± 0.06	4.22 ± 0.07	4.23 ± 0.07	2.29
14	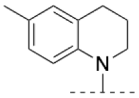	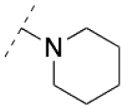	4.61 ± 0.06	4.75 ± 0.08	4.73 ± 0.07	4.18 ± 0.09	4.67 ± 0.07	3.74
15	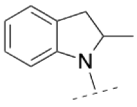	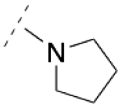	< 4	4.00 ± 0.08	4.67 ± 0.05	4.10 ± 0.08	4.13 ± 0.08	2.79
16	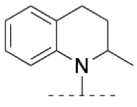	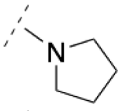	5.31 ± 0.07	4.35 ± 0.07	5.61 ± 0.05	< 4	5.20 ± 0.05	3.20
17	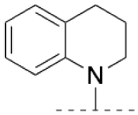	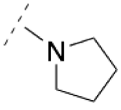	6.21 ± 0.06	5.54 ± 0.04	6.41 ± 0.05	5.13 ± 0.07	5.86 ± 0.06	2.68
18	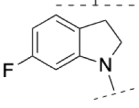	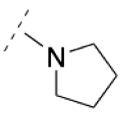	4.12 ± 0.06	< 4	4.30 ± 0.07	4.02 ± 0.09	< 4	2.59
19	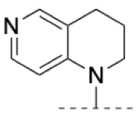	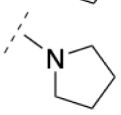	< 4	4.03 ± 0.10	4.36 ± 0.09	4.07 ± 0.08	< 4	1.73

Value denoted as Mean ± SEM.

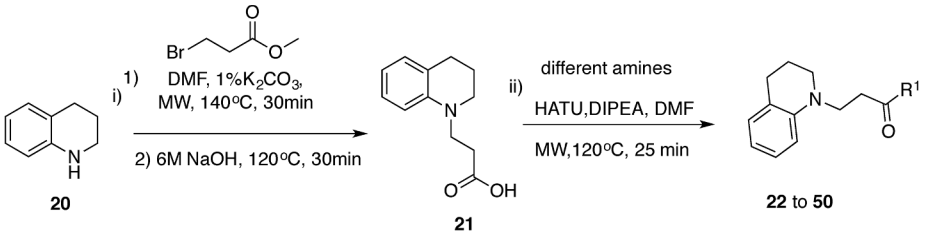

Scheme 2. Synthetic approach for the ligand optimization to setup the focused library 2. i) 1) DMF, 1% K_2CO_3, MW, 140 °C, 30 min; 2) 6 M NaOH, MW, 120 °C, 30 min; ii) HATU, DIPEA, DMF, MW, 120 °C, 25 min.

Table 2

Structure and activity of the focused library 2.

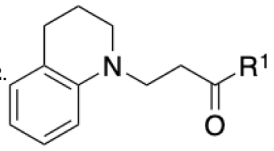

Entry	R^1	pIC50 M2	pKi M1	pKi M2	pKi M3	pKi M4	cLogP
22	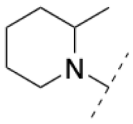	5.50 ± 0.06	5.20 ± 0.06	5.49 ± 0.06	5.07 ± 0.07	5.28 ± 0.07	3.86
23	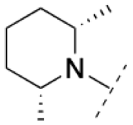	5.62 ± 0.07	5.94 ± 0.07	5.95 ± 0.09	5.45 ± 0.07	5.95 ± 0.05	4.38
24	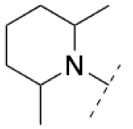	4.66 ± 0.07	4.56 ± 0.05	5.32 ± 0.08	4.26 ± 0.06	4.75 ± 0.07	4.38
25	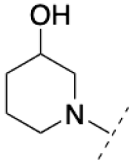	4.53 ± 0.07	4.48 ± 0.04	5.21 ± 0.06	4.27 ± 0.06	4.73 ± 0.04	1.87
26	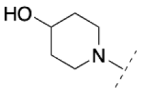	4.82 ± 0.08	4.63 ± 0.03	4.88 ± 0.07	4.48 ± 0.06	4.77 ± 0.04	1.52
27	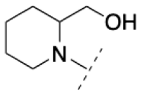	4.97 ± 0.05	4.94 ± 0.04	5.44 ± 0.05	4.50 ± 0.05	5.14 ± 0.04	2.29
28	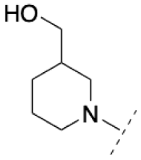	6.12 ± 0.07	5.84 ± 0.05	6.21 ± 0.04	5.28 ± 0.05	5.76 ± 0.04	2.29
29	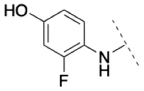	< 4	< 4	4.19 ± 0.09	< 4	< 4	3.29
30	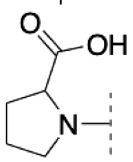	6.11 ± 0.07	5.98 ± 0.06	6.24 ± 0.10	5.34 ± 0.05	6.05 ± 0.05	3.00
31	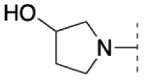	4.15 ± 0.10	4.29 ± 0.05	4.78 ± 0.06	< 4	4.30 ± 0.03	1.90

(*continued on next page*)

Table 2 (*continued*)

Entry	R^1	pIC50 M2	pKi M1	pKi M2	pKi M3	pKi M4	cLogP
32	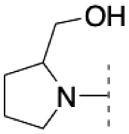	4.72 ± 0.07	4.85 ± 0.04	5.29 ± 0.06	4.49 ± 0.08	4.93 ± 0.05	2.52
33	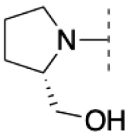	4.76 ± 0.05	4.85 ± 0.03	5.29 ± 0.07	4.36 ± 0.09	4.89 ± 0.03	2.52
34	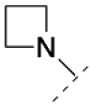	4.92 ± 0.05	5.35 ± 0.05	5.77 ± 0.05	4.94 ± 0.08	5.24 ± 0.06	2.23
35	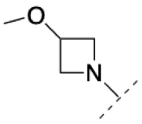	4.69 ± 0.04	4.76 ± 0.03	5.45 ± 0.06	4.49 ± 0.07	4.80 ± 0.07	3.34
36	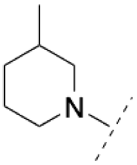	5.82 ± 0.05	6.22 ± 0.07	6.39 ± 0.07	5.54 ± 0.07	6.11 ± 0.06	3.86
37	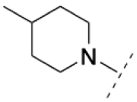	6.25 ± 0.05	6.52 ± 0.07	7.05 ± 0.07	6.01 ± 0.07	6.54 ± 0.04	3.86
38	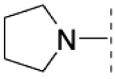	5.74 ± 0.07	5.98 ± 0.05	6.54 ± 0.07	5.54 ± 0.06	5.80 ± 0.06	2.78
39	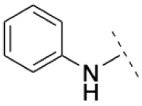	6.27 ± 0.07	6.58 ± 0.06	6.94 ± 0.04	6.11 ± 0.09	6.67 ± 0.06	4.04
40	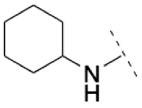	6.53 ± 0.06	6.64 ± 0.05	7.26 ± 0.04	5.76 ± 0.05	6.80 ± 0.04	4.11
41	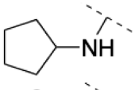	6.50 ± 0.06	6.61 ± 0.05	7.01 ± 0.05	5.59 ± 0.06	6.59 ± 0.04	3.55
42	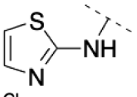	6.40 ± 0.05	5.95 ± 0.06	5.46 ± 0.08	< 4	4.23 ± 0.77	3.28
43	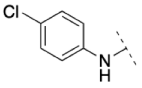	5.85 ± 0.06	5.25 ± 0.04	5.48 ± 0.05	4.97 ± 0.07	4.97 ± 0.06	5.01
44	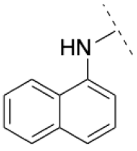	6.47 ± 0.07	5.03 ± 0.03	6.04 ± 0.05	4.58 ± 0.14	5.39 ± 0.10	5.22
45	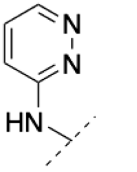	5.18 ± 0.05	4.85 ± 0.05	5.14 ± 0.06	4.53 ± 0.08	4.85 ± 0.06	2.56

(*continued on next page*)

Table 2 (*continued*)

Entry	R^1	pIC50 M2	pKi M1	pKi M2	pKi M3	pKi M4	cLogP
46	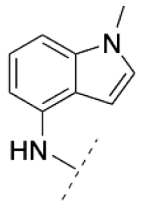	6.37 ± 0.06	5.30 ± 0.06	5.64 ± 0.09	< 4	4.92 ± 0.09	4.71
47	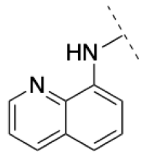	6.32 ± 0.07	5.31 ± 0.05	6.21 ± 0.08	< 4	4.74 ± 0.10	4.55
48	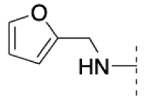	5.95 ± 0.07	5.58 ± 0.04	5.91 ± 0.05	4.92 ± 0.07	5.36 ± 0.05	3.18
49	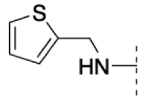	5.99 ± 0.06	6.19 ± 0.05	6.19 ± 0.04	5.14 ± 0.05	5.67 ± 0.05	3.65
50	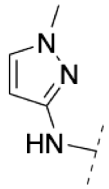	6.01 ± 0.07	5.12 ± 0.05	5.48 ± 0.05	4.59 ± 0.09	5.06 ± 0.06	2.56
51	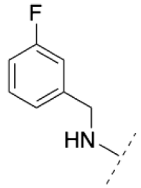	5.86 ± 0.07	5.69 ± 0.04	5.72 ± 0.07	4.89 ± 0.11	5.19 ± 0.04	4.15

Value denoted as Mean ± SEM.

comparison between **8**, **10**, **11**, **13** and **15**, **16**, **17**, **19**. For this initial optimization, we discovered two novel ligands (**11** and **17**) featuring a 100-fold higher IC_{50} compared to the lead compound **1**. The result of the IC_{50} in Table 1 also indicates the substitution of carbazole with tetrahydroquinoline will dramatically improve the IC_{50} of the scaffold.

In order to discover the novel ligands with higher M_2 drug potential, binding affinity and specificity, further optimization with **11** was also performed using the synthetic approach shown in Scheme 2. In this optimization, we took the linker length of ACh into accounts and elongated the linker between the tetrahydroquinoline and the amine from 2-carbon to 3-carbon. Furthermore, we also employed a variety of amines for the construction of a novel focused library as shown in Table 2. By analyzing the M_2 IC_{50} of the compounds in this focused library, we discovered several novel ligands featuring the sub-micromolar binding IC_{50}, like **28, 30, 37, 39, 40, 41, 42, 44, 46, 47** and **50** as shown in Table 2. Direct comparison between data in Table 1 and Table 2 indicates the 3-carbon linker between the tetrahydroquinoline group and the amine groups has an equivalent drug potential and binding affinities for M_1 to M_4 when compared with the two-carbon linker, as indicated by ligands of **17** and **38**. In sum, the second-round optimization of the scaffold in Table 2 offers a variety of novel M_2 subtype ligands with an overall increased mAChRs binding affinity and M_2 IC_{50} when compared to the ligands in Table 1.

Since the ligands showed antagonism toward M2 mAChR, they could be antagonists or NAMs. For NAMs, they could shift ACh titration curve to the right in radioligand binding assay; while it would not happen for antagonists. By using ACh titration in absence/presence of 100 μM **8**, **15** and **47**, it was identified that these ligands were antagonists, rather than NAMs (data not shown). In order to elucidate the binding specificity for each ligand, the binding affinities to each subtype (M_1 to M_4) in Table 1 and Table 2 were also analyzed. The M5 mAChR-expressing cell line was provided by our vender GenScript and it exhibited quite low expression level, which made us difficult to characterize.

The inhibition constant, Ki, is reflective of the binding affinity and could be determined with radioligand competition binding assays. In the assay, both ACh and atropine were taken as positive controls for competitive binding and showed pKi as follows: M_1: 4.3 (ACh) and 9.5 (atropine), M_2: 5.6 (ACh) and 8.5 (atropine), M_3: 4.5 (ACh) and 9.0 (atropine), M_4: 4.9 (ACh) and 9.0 (atropine). As shown in Fig. 3, by directly comparing the pKi values for M_2 with the other three mAChR subtypes, we can directly determine the binding specificity for each compound. In detail, the binding specificity for M_2 over M_1, M_3 and M_4 was determined individually for each compound using the pKi values calculated. By comparing M_2 and M_1 binding affinity, we noticed ligands **9**, **10**, **16, 17, 44** and **47** demonstrate a significant higher (~8-fold) binding affinity for M_2 over M_1, as shown in Fig. 3**A**. While for M_2 over M_3 selectivity, ligands **16**, **42** and **47** demonstrate more than 50-fold higher binding specificity, as shown in Fig. 3**B**. For M_2 over M_4 selectivity, only ligands **42** and **47** demonstrates more than 16-fold higher binding selectivity as shown in Fig. 3**C**. The binding curve in Fig. 4**A** and Fig. 4**C** clearly demonstrate ligand **47** binds specificity to

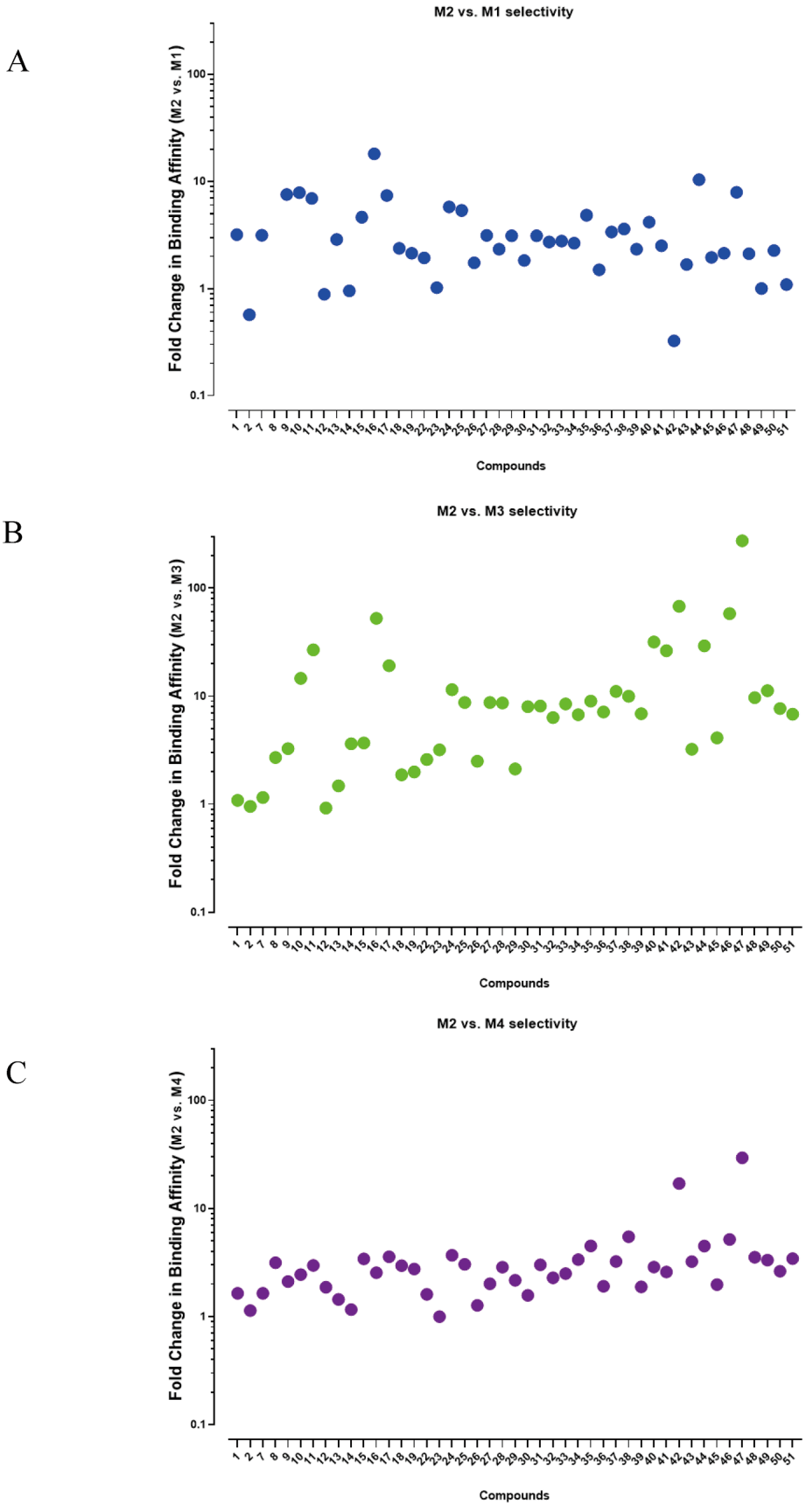

Fig. 3. The binding affinity comparison among different mAChRs. (A) The binding affinity comparison between M2 and M1 subtypes for all the ligands; (B) The binding affinity comparison between M2 and M3 subtypes for all the ligands; (C) The binding affinity comparison between M2 and M4 subtypes for all the ligands.

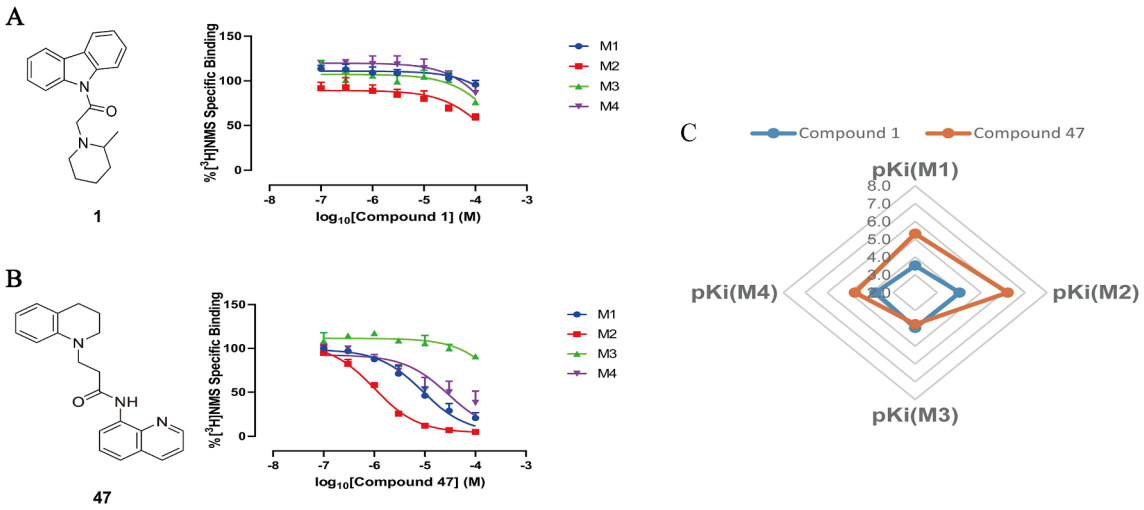

Fig. 4. Comparison between lead compound **1** and novel M_2 antagonist **47** on their mAChRs subtype selectivity. (A) mAChRs selectivity for compound **1**; (B) mAChRs selectivity for compound **47**; (C) Binding selectivity comparison between **1** and **47**.

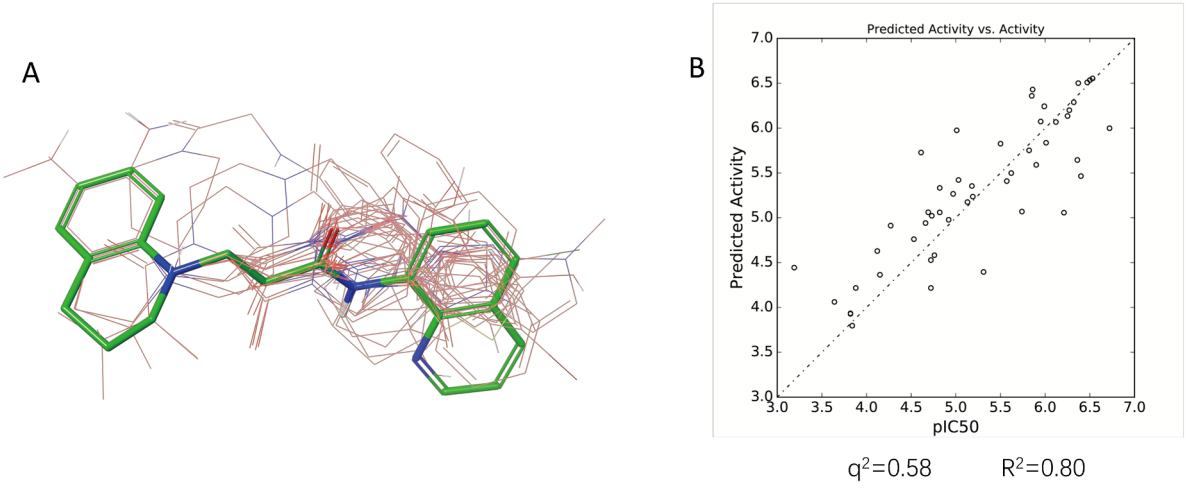

Fig. 5. The evaluation of QSAR performance (A) Scaffold alignment for all the ligands; (B) Experimental vs predicted biological activities.

M_2 when compared to the other subtypes of mAChRs. To the contrary, the lead compound **1** did not show a specific binding profile as compound **47**, as shown in Fig. 4A, 4B, and 4C. In summary, the novel ligand **47** features an 8-fold higher binding affinity than M_1, more than 250-fold higher binding affinity than M_3 and ~30-fold higher than M_4, demonstrating a significant selectivity for M_2 subtype as shown in Fig. 3 and Fig. 4.

The cLogP measurement using ChemDraw (Perkin Elmer, USA) was also performed to evaluate the lipophilicity for each compound. The result indicates the lead compound **1** has a higher lipophilicity (cLogP = 5.45) when compared with most of the compounds in Table 1 and Table 2, with a cLogP in a range of 1.5 to 5.5. The desired compound **47** also has a lipophilicity with cLogP equals 4.55, which is in a suitable range of 3 to 5.

The quantitative structure–activity relationships (QSAR) model was generated based on best conformations and common substructure alignment. The retrieved conformations of all the molecules from LigPrep module were superimposed using the common scaffold alignment approach of Schrödinger Suite (Fig. 5**A**). The training set of 30 molecules was randomly selected to build the model. The best model (PLS factor = 3) offered a good predictive power. The leave-one-out (LOO) method of cross-validation was adopted for assessment of the predictive abilities of the models. The R^2 for the regression was 0.7913 and the stability was 0.7210. The p value (5.34 e −-9) also suggested a greater degree of confidence. Since external test was the gold standard for QSAR model validation, the reliability of the model was tested by external test set of 20 compounds. According to the recommended rules for robust model,[35] the RMSE (0.58), Q^2 (0.6121) and Pearson's r (0.8048) of the model all further confirmed its robustness. Correlation between the experimental and predicted activities for the data set is displayed in Fig. 5**B**.

The five conventional Gaussian fields, which contained Gaussian steric, electrostatic, hydrophobic, H-bond acceptor and H-bond donor field, illustrated that the substituents on far-end aromatic ring and near-end aromatic ring were crucial for the activity. To depict the field-based QSAR model in detail, the compound **47** was placed in the field contour maps as reference ligand.

From the steric and electrostatic contour map (Fig. 6**A**), we could observe that one kidney-like region exists at the center of near-end aromatic ring as illustrated with green contour parts. Thus, the introduction of a bulky moiety on amide carbonyl group would improve the inhibitory activity, as was shown on the compound **34**

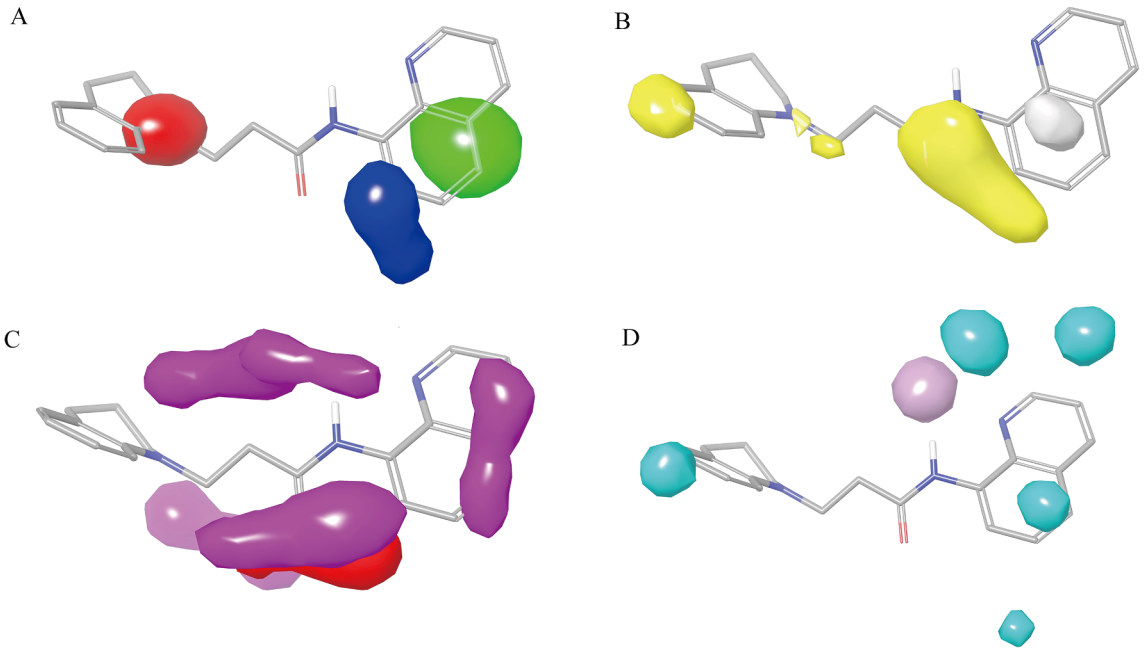

Fig. 6. Field-based QSAR models for the ligands (A) Gaussian steric field: Green (+) and Gaussian electrostatic field: Blue (+), Red (−); (B) Gaussian hydrophobic field: Yellow (+), White (−); (C) Gaussian hbond acceptor field: Red (+), Magenta (−); (D) Gaussian hbond donor field: Purple (+), Cyan (−). (For interpretation of the references to colour in this figure legend, the reader is referred to the web version of this article.)

(pIC_{50} = 4.92) and the compound **40** (pIC_{50} = 6.53). Besides, the size of the substitution was not strictly limited. Although the dual aromatic ring was rigid and larger, the activity was not significantly decreased, which could be observed on the compound **40** (pIC_{50} = 6.53) and the compound **44** (pIC_{50} = 6.47).

From the electrostatic field contour map (Fig. 6**A**), we noticed that electropositive group, with blue contour part, at the near-end aromatic ring might contribute to the activity. The red contour at far-end nitrogen indicated that introducing electronegative group or electron donating group substitution on this aromatic ring would potentially improve the activity. For example, the compound **9** (pIC_{50} = 5.03) bearing with hydroxyl group substitution could be more active than that of compound **18** with fluoro-substitution (pIC_{50} = 4.12).

The hydrophobicity contour map, presented in Fig. 6**B**, is consistent with the hydrophobicity of the aromatic lid of M_2 receptor, which clearly demonstrated that the amide-aromatic ring area and the far-end aromatic area were in the solvent-inaccessible hydrophobic pocket. The yellow contour (Fig. 6**B**) around these two positions was recognized as a preference for the hydrophobic group as described in the interaction mode from docking. The introduction of the hydrophilic moiety at either region could result in decreased activity. This trend could be seen from the compound **11** (pIC_{50} = 6.36) VS **13** (pIC_{50} = 3.19) and **25** (pIC_{50} = 4.53), respectively.

The red contour maps at the amide carbonyl group showed the importance of oxygen atom as H-bond acceptor. The magenta contour maps around linker suggested that H-bond acceptors were disfavored at these places (Fig. 6**C**). The purple contour in Fig. 6**D** suggested that H-bond donor groups would be beneficial to the amide nitrogen. For example, the H-bond was observed between amide nitrogen and hydroxyl group of Tyr104 side chain, which was vital for the combination of the ligands with M_2 receptor. Besides, the cyan contour maps around the compound showed that H-bond donors were disfavored, which could be accordant with the hydrophobic maps. Therefore, field contribution of the defined features in the final model revealed that H-bond donor field was the fundamental for the activity and steric field, hydrophobic field contributed the most to the activity regulation.

Compounds **47** was docked to the orthosteric binding site of the human M_2 receptor X-ray structure in the inactive state in complex with quinuclidinyl benzylate (QNB) (PDB ID: 3UON). The molecular docking was performed with the standard precision (SP) approach of Glide in Schrödinger Suite with default settings using the grid based on the cocrystallized ligand, QNB. The selected binding pose and interaction diagram of compound **47** are shown in Fig. 7. The main contact of compound **47** with the human muscarinic M_2 receptor is a hydrogen bond interaction between the amide nitrogen of the ligand and the conserved Tyr104 (3.33) (Ballesteros–Weinstein nomenclature) from the third transmembrane helix, as is typical for orthosteric ligands of aminergic GPCRs. Moreover, there is pi-pi stacking interaction between the far-end aromatic ring of the core amide group and the side chain of Tyr104. In our model, there was no strong interaction with the known key residues (Asp103 and Asn404) for other ligands, e.g. AFDX 384, which indicated that these ligands could bind to a partially different orthosteric site. That could be why the affinity of our ligands were much lower than AFDX 384 and it was confirmed that compound 47 had a different pose from AFDX 384, when comparing the docking model with the crystal structure of M_2-AFDX 384 complex (PDB ID: 5ZKB).[15]

Because Phe181 was the specific residue, which was only located around the orthosteric site of M_2 subtype, we considered that Phe181 should play important roles in the selectivity of compound **47**. The aromatic ring at the near-end of the amide group is surrounded by the famous aromatic lid, including Tyr403, Phe181 and Tyr177 (Fig. 7**A and 7B**). The aromatic lid could change the binding kinetics for both association and dissociation, which was also accordant with the faster kinetics of M_2 subtype in radioligand binding assay. Comparing to the interactions of non-selective QNB and tiotropium,[29,33,36] interactions with aromatic lid in M_2 receptor could allow the accommodation of bulkier ligand and the bulkier moiety could contribute to the selectivity, which has been confirmed in another new M_2-selective antagonist with crystal structures.[15]

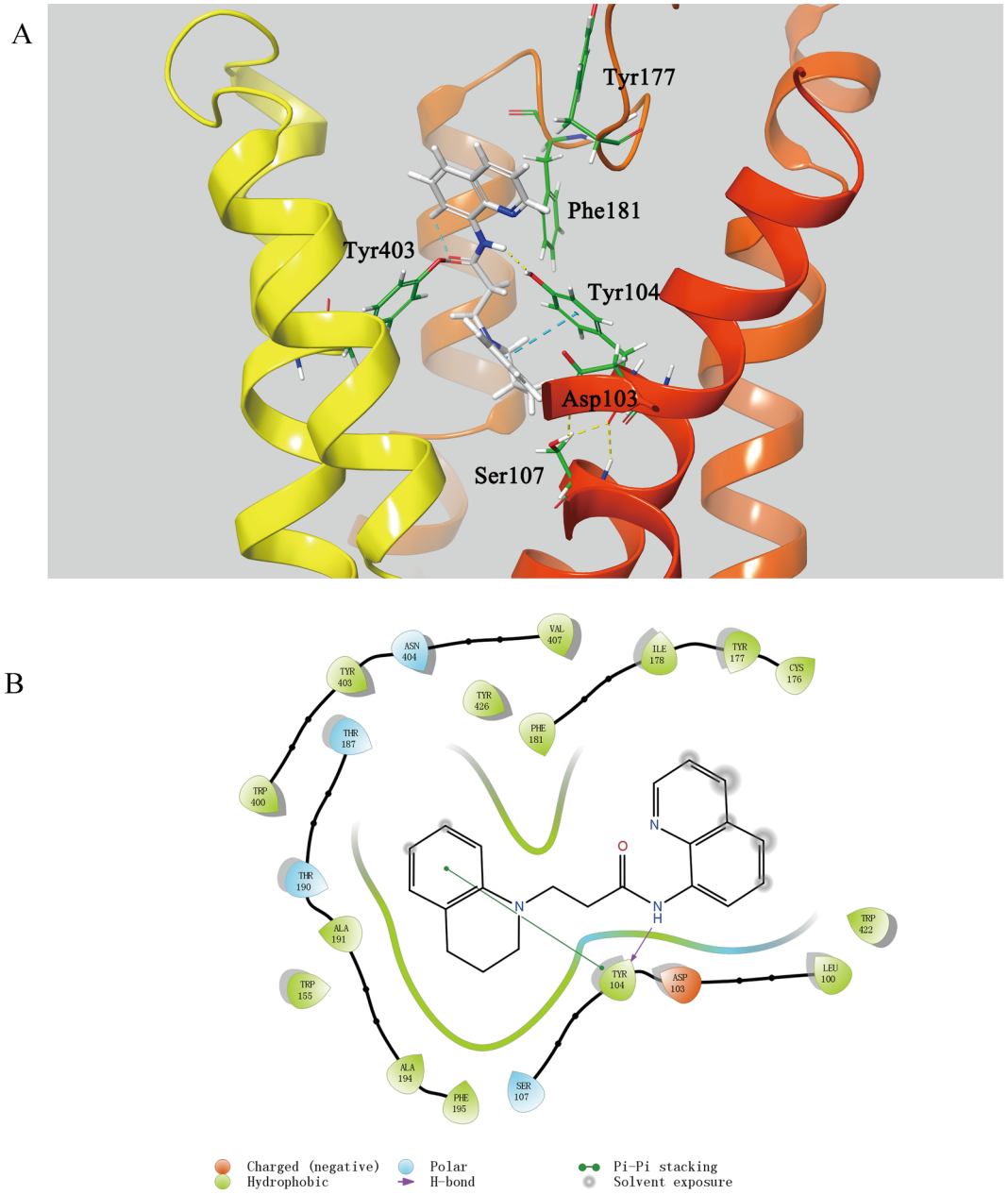

Fig. 7. Interaction model of compound **47** and M2 subtype.

In conclusion, by using virtual screening, we discovered a novel lead compound featuring a specific binding and potential to mAChRs. The following optimization based on this scaffold yielded a class of novel ligands featuring submicromolar IC_{50} for M_2 subtype. Among these, ligand **47** exhibits a specific M_2 binding selectivity and high drug potential (IC_{50}). Furthermore, the binding affinity, potential and QSAR obtained from this study will also give the valuable information in further development of M_2 subtype ligands.

Declaration of Competing Interest

The authors declare that they have no known competing financial interests or personal relationships that could have appeared to influence the work reported in this paper.

Acknowledgments

This work was supported by National Natural Science Foundation of China (81601536 to Dewei Tang, 81503174 to Jianrong Xu, 81973297 to Hao Wang and 81872841 to Hongzhuan Chen) and by Shanghai Committee of Science and Technology (19JC1413100 to Hao Wang).

Appendix A. Supplementary data

Supplementary data to this article can be found online at https://doi.org/10.1016/j.bmcl.2020.127632.

References

1. Hauser AS, Chavali S, Masuho I, et al. Pharmacogenomics of GPCR drug targets. *Cell.* 2018;172:41–54 e19.

2. Wess J, Eglen RM, Gautam D. Muscarinic acetylcholine receptors: mutant mice provide new insights for drug development. *Nat Rev Drug Discov.* 2007;6(9):721–733.
3. VanPatten S, Al-Abed Y. The challenges of modulating the 'rest and digest' system: acetylcholine receptors as drug targets. *Drug Discov Today.* 2017;22(1):97–104.
4. Moran SP, Maksymetz J, Conn PJ. Targeting muscarinic acetylcholine receptors for the treatment of psychiatric and neurological disorders. *Trends Pharmacol Sci.* 2019;40(12):1006–1020.
5. Kruse AC, Kobilka BK, Gautam D, Sexton PM, Christopoulos A, Wess J. Muscarinic acetylcholine receptors: novel opportunities for drug development. *Nat Rev Drug Discov.* 2014;13(7):549–560.
6. Thomsen M, Sørensen G, Dencker D. Physiological roles of CNS muscarinic receptors gained from knockout mice. *Neuropharmacology.* 2018;136(Pt C):411–420.
7. Valuskova P, Farar V, Forczek S, Krizova I, Myslivecek J. Autoradiography of 3H-pirenzepine and 3H-AFDX-384 in Mouse Brain Regions: possible insights into M1, M2, and M4 muscarinic receptors distribution. *Front Pharmacol.* 2018;9:124.
8. Korczynska M, Clark MJ, Valant C, et al. Structure-based discovery of selective positive allosteric modulators of antagonists for the M2 muscarinic acetylcholine receptor. *Proc Natl Acad Sci.* 2018;115(10):E2419–E2428.
9. Greenlee W, Clader J, Asberom T, et al. Muscarinic agonists and antagonists in the treatment of Alzheimer's disease. *Farmaco.* 2001;56(4):247–250.
10. Rowe WB, O'Donnell JP, Pearson D, Rose GM, Meaney MJ, Quirion R. Long-term effects of BIBN-99, a selective muscarinic M2 receptor antagonist, on improving spatial memory performance in aged cognitively impaired rats. *Behav Brain Res.* 2003;145(1–2):171–178.
11. Muramatsu I, Uwada J, Yoshiki H, et al. Novel regulatory systems for acetylcholine release in rat striatum and anti-Alzheimer's disease drugs. *J Neurochem.* 2019;149(5):605–623.
12. Jakubik J, El-Fakahany EE. Current advances in allosteric modulation of muscarinic receptors. *Biomolecules.* 2020;10(2) pii: E325.
13. Bock A, Schrage R, Mohr K. Allosteric modulators targeting CNS muscarinic receptors. *Neuropharmacology.* 2018;136(Pt C):427–437.
14. Liu H, Hofmann J, Fish I, et al. Structure-guided development of selective M3 muscarinic acetylcholine receptor antagonists. *Proc Natl Acad Sci.* 2018;115(47):12046–12050.
15. Suno R, Lee S, Maeda S, et al. Structural insights into the subtype-selective antagonist binding to the M2 muscarinic receptor. *Nat Chem Biol.* 2018;14(12):1150–1158.
16. Del Bello F, Bonifazi A, Quaglia W, et al. Mode of interaction of 1,4-dioxane agonists at the M2 and M3 muscarinic receptor orthosteric sites. *Bioorg Med Chem Lett.* 2014;24(15):3255–3259.
17. Del Bello F, Bonifazi A, Giorgioni G, et al. Novel potent muscarinic receptor antagonists: investigation on the nature of lipophilic substituents in the 5- and/or 6-positions of the 1,4-dioxane nucleus. *J Med Chem.* 2020;63(11):5763–5782.
18. Lachowicz JE, Duffy RA, Ruperto V, et al. Facilitation of acetylcholine release and improvement in cognition by a selective M2 muscarinic antagonist, SCH 72788. *Life Sci.* 2001;68(22–23):2585–2592.
19. Quirion R, Wilson A, Rowe W, et al. Facilitation of acetylcholine release and cognitive performance by an M(2)-muscarinic receptor antagonist in aged memory-impaired. *J Neurosci.* 1995;15(2):1455–1462.
20. Doods H, Entzeroth M, Ziegler H, et al. Characterization of BIBN 99: a lipophilic and selective muscarinic M2 receptor antagonist. *Eur J Pharmacol.* 1993;242(1):23–30.
21. Hernandez CM, Terry Jr AV. Repeated nicotine exposure in rats: effects on memory function, cholinergic markers and nerve growth factor. *Neuroscience.* 2005;130(4):997–1012.
22. Pittel Z, Lazar S, Gez R, Chapman S. Early changes in M2 muscarinic acetylcholine receptors (mAChRs) induced by sarin intoxication may be linked to long lasting neurological effects. *Neurotoxicology.* 2018;65:248–254.
23. Watson N, Barnes PJ, Maclagan J. Actions of methoctramine, a muscarinic M2 receptor antagonist, on muscarinic and nicotinic cholinoceptors in guinea-pig airways in vivo and in vitro. *Br J Pharmacol.* 1992;105(1):107–112.
24. Wess J, Angeli P, Melchiorre C, Moser U, Mutschler E, Lambrecht G. Methoctramine selectively blocks cardiac muscarinic M2 receptors in vivo. *Naunyn Schmiedebergs Arch Pharmacol.* 1988;338(3):246–249.
25. Jakubík J, Zimčík P, Randáková A, Fuksová K, El-Fakahany EE, Doležal V. Molecular mechanisms of methoctramine binding and selectivity at muscarinic acetylcholine receptors. *Mol Pharmacol.* 2014;86(2):180–192.
26. Gamberini MT, Bolognesi ML, Nasello AG. The modulatory role of M2 muscarinic receptor on apomorphine-induced yawning and genital grooming. *Neurosci Lett.* 2012;531(2):91–95.
27. Chiarini A, Budriesi R, Bolognesi ML, Minarini A, Melchiorre C. In vitro characterization of tripitramine, a polymethylene tetraamine displaying high selectivity and affinity for muscarinic M2 receptors. *Br J Pharmacol.* 1995;114(7):1507–1517.
28. Angeli P, Cantalamessa F, Gulini U, Melchiorre C. Selective blockade of muscarinic M2 receptors in vivo by the new antagonist tripitramine. *Naunyn Schmiedebergs Arch Pharmacol.* 1995;352(3):304–307.
29. Haga K, Kruse AC, Asada H, et al. Structure of the human M2 muscarinic acetylcholine receptor bound to an antagonist. *Nature.* 2012;482(7386):547–551.
30. Kruse AC, Ring AM, Manglik A, et al. Activation and allosteric modulation of a muscarinic acetylcholine receptor. *Nature.* 2013;504(7478):101–106.
31. Staus DP, Hu H, Robertson MJ, et al. Structure of the M2 muscarinic receptor–β-arrestin complex in a lipid nanodisc. *Nature.* 2020;579(7798):297–302.
32. Thal DM, Sun B, Feng D, et al. Crystal structures of the M1 and M4 muscarinic acetylcholine receptors. *Nature.* 2016;531(7594):335–340.
33. Vuckovic Z, Gentry PR, Berizzi AE, et al. Crystal structure of the M5 muscarinic acetylcholine receptor. *Proc Natl Acad Sci.* 2019;116(51):26001–26007.
34. Maeda S, Qu Q, Robertson MJ, Skiniotis G, Kobilka BK. Structures of the M1 and M2 muscarinic acetylcholine receptor/G-protein complexes. *Science.* 2019;364(6440):552–557.
35. Cappel D, Dixon SL, Sherman W, Duan J. Exploring conformational search protocols for ligand-based virtual screening and 3-D QSAR modeling. *J Comput Aided Mol Des.* 2015;29(2):165–182.
36. Burger WA, Sexton PM, Christopoulos A, Thal DM. Toward an understanding of the structural basis of allostery in muscarinic acetylcholine receptors. *J Gen Physiol.* 2018;150(10):1360–1372.